CHAPTER III

RESULTS AND DISCUSSION

We achieved the calculation on the five target initiators namely, tin(II)-*n*-butoxide: $Sn(O\text{-}nBut)_2$, tin(II)-*iso*-butoxide: $Sn(O\text{-}iBut)_2$, tin(II)-*tert*-butoxide: $Sn(O\text{-}tBut)_2$, tin(II)-hexoxide: $Sn(O\text{-}nHex)_2$, tin(II)-octoxide: $Sn(O\text{-}nOct)_2$. We have calculated geometries, energies and vibrational frequencies of all stationary points (reactant, transition state, intermediate and product) along the reaction profiles of ring-opening polymerization (ROP) between the ε-caprolactone (CL) and tin(II) alkoxide initiator. We followed the six steps of ROP mechanism as depicted in Figure 1.7 of chapter 1. All calculations were performed using hybrid density functional theory (DFT) at B3LYP level with mixed basis set. For metal atom, a doublet-ζ-valence quality basis set LANLD2Z is assigned for Sn atom. A relativistic electron core potential (ECP) is developed by Hay and Wadt replaced the Sn core electron. For non-metal atom, a valence triple zeta with polarization function (VTZ2P) at cc-pVTZ is assigned for C, H, and O atoms.

In this chapter, the calculated information will be analyzed and discussed in three main topics such as geometry optimization, energy minimization and kinetics rate reaction. The results from theoretical study may be supported with the experimental results and they may be useful for explaining the details information on the polymer catalyst.

3.1 Geometry optimization

3.1.1 Structure mechanism analysis

Many literatures and also conclusion from Manita *et al.* [13] suggested that the good method to synthesize the poly(ε-caprolactone) (PCL) with high percent yield was achieved by coordination-insertion mechanism of ROP method in bulk of the CL using tin(II) alkoxide initiators. And the new mechanism was also proposed clearly (step-by-step) in Figure 1.7. For specific calculation, each states of mechanism were labeled in Figure 3.1.

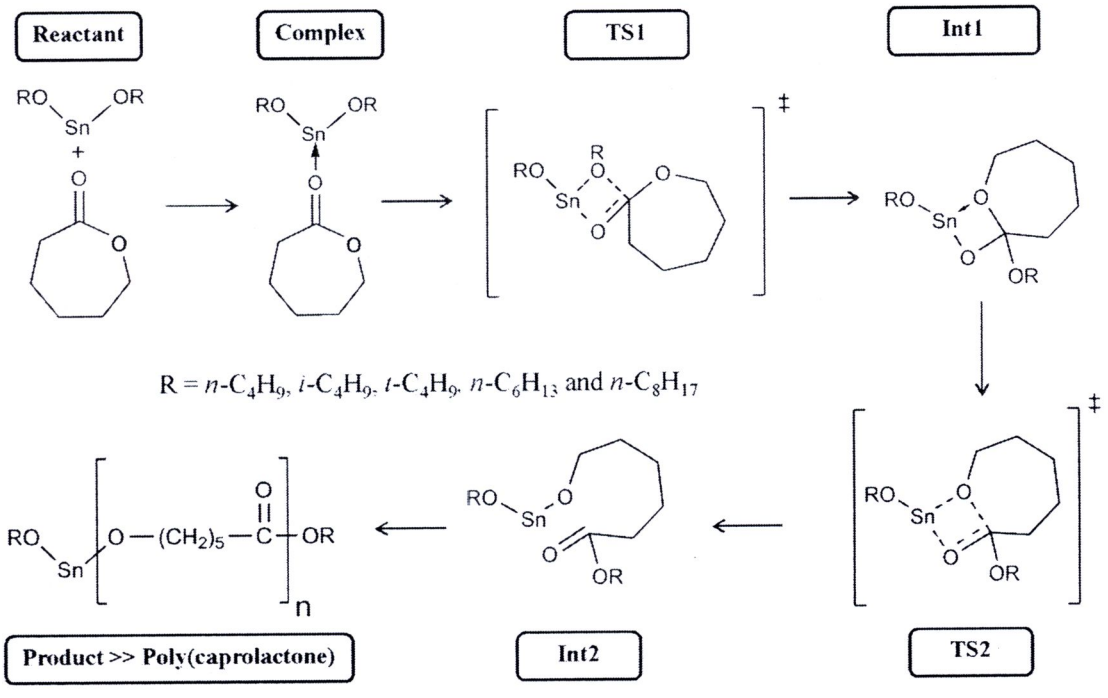

Figure 3.1 The structural mechanism in each state of ROP of CL initiated by tin(II) alkoxides using in this calculation

According to the geometry information (geometries, energies and vibrational frequencies), our results support a coordination-insertion mechanism initiated by tin(II) alkoxides with two transition states and seven states of reaction prior to the

ROP (**Reactant**, **Complex**, **TS1**, **Int1**, **TS2**, **Int2**, **Product**). The detailed information on the ROP mechanism is described in the following six steps:

I. **Complex**: In the initial step involves the weak complexation of CL and tin(II)-alkoxide. The weak complex can be formed by a coordination interaction between CL and tin(II)-alkoxide initiator . An electrophilic attack by carbonyl group of CL onto the nucleophilic Sn atom of tin(II)-alkoxide is attained.

II. **Transition state 1** (**TS1**): The second step is the first transition state formation. This four-membering transition state is formed by introducing the new bond between Sn and oxygen atom on the carbonyl group of CL.

III. **Intermediate 1** (**Int1**): The third step is the stable intermediate formation. This intermediate is formed by rotating the alkoxyl (-OR) group away from the Sn atom and the weak interaction between Sn and oxygen atom from is attained.

IV. **Transition state 2** (**TS2**): The forth step involves the formation of second transition state. This transition state can be achieved by making a covalent bond of Sn atom to the oxygen atom adjacent to the carbonyl group. The high constraint four-membering transition is readily to open the CL forming the product.

V. **Intermediate 2** (**Int2**): This step concern about **TS2** eventually ruptures to **Int2** resulting in increasing bond length of C^1-O^1 before propagation to product.

VI. **Product**: The final step is the product formation. This product is the consequence of ring-opening of **TS2** species. The second monomer of CL

can be added into this product and the propagation of next ROP is continued.

The structural details of all reactions (bond distance and energy formation) from geometry optimization are discussed in the next section in the order of tin(II) alkoxide initiators: $Sn(O\text{-}nBut)_2$, $Sn(O\text{-}nHex)_2$, $Sn(O\text{-}nOct)_2$, $Sn(O\text{-}iBut)_2$, and $Sn(O\text{-}tBut)_2$, respectively.

3.1.1.1 $Sn(O\text{-}nBut)_2$

The tin(II)-*n*-butoxide assisted ROP coordination-insertion mechanism for monomer of CL was investigated by DFT(B3LYP) with mix basis set method. The corresponding DFT based optimized structures and energies of each step followed Figure 3.1. The exo-carbonyl group of CL coordinates the Sn metal (**Complex**) with O^1 in the *cis* position, resulting in a Sn-O^2 distance of 2.61 Å. The energy of complex formation is -7.53 kcal mol^{-1}. The transformation of **Complex** into **TS1** involves addition of the Sn-O^3 onto the C^1-O^2 double bond and a corresponding rotation of the O^1-C^1-O^2 plane 90° forming a planar four-membered ring (**TS1**) having sp^2-sp^3 hybridized C^1 which is located above that O^2-C^1-O^1 plane. This process lengthens the Sn-O^3 and shortens the Sn-O^2 (Figure 3.2). This process requires moderate energy (14.58 kcal mol^{-1}) and the supported DFT with only one negative imaginary frequency is confirmed.

The conversion of **TS1** to intermediate1 (**Int1**) involves rotation of CL ring around the C^1-O^2 bond resulting in a decrease and increase in the Sn-O^3 and Sn-O^1 distances respectively (Figure 3.2). The Sn-O^1 distance is about 3.41 Å which is not a bond between but only attractive force between the two atoms.

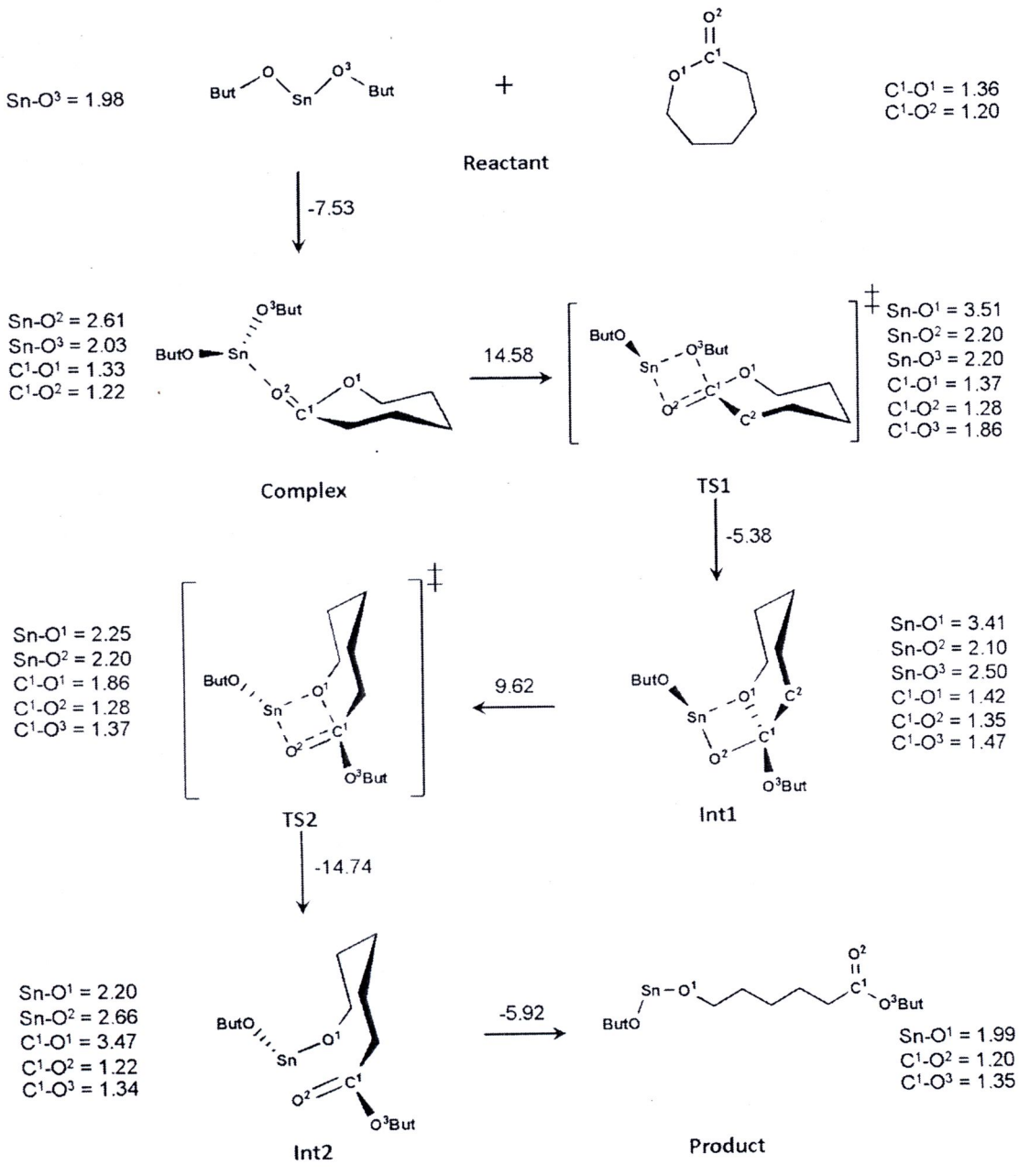

Figure 3.2 ROP mechanism of CL initiated with $Sn(O\text{-}nBut)_2$. Bond lengths are in Å and energies formation are in kcal mol^{-1}

The **Int1** energy is 9.2 kcal mol^{-1} above the **Complex**. The optimized transition state 2, **TS2**, shows a four-membered ring with nearly equal $Sn\text{-}O^1$ and $Sn\text{-}O^2$ distance and a sp^3 hybridized C^1 atom with $C^1\text{-}O^1$, $C^1\text{-}O^2$ and $C^1\text{-}O^3$ bond lengths between 1.28 and 1.86 Å. This step is completely attained when the bond of $Sn\text{-}O^1$ is

created. The **TS2** structure is confirmed by an imaginary frequency and intrinsic reaction coordination (IRC) calculation indicating that saddle point along the reaction pathway is exists. This **TS2** eventually ruptures to intermediate2 (**Int2**) and then form **Product** with increasing bond length of C^1-O^1. Our DFT based calculation gave two transition state formation steps with the **TS1** being as the rate-determining step. Our calculated results based on proposed mechanism in Figure 3.1 of tin(II)-*n*-butoxide with CL is found similar to the proposed ROP mechanism of $SnMe_3OMe$ with 1,5-dioxepan-2-one (DXO) reported by von Schenck and co-workers [21]. This may be due to the similarity of coordinate stability for Sn both in tetravalent and divalent forms. The overall reaction is exothermic.

And for the other initiators, The ROP mechanism of CL with other tin(II) alkoxides ($Sn(OR)_2$) namely: $Sn(O\text{-}nHex)_2$ in Figure3.3, $Sn(O\text{-}nOct)_2$ in Figure 3.4, $Sn(O\text{-}iBut)_2$ in Figure 3.5, and $Sn(O\text{-}tBut)_2$ in Figure 3.6 are similar to that of CL with $Sn(O\text{-}nBut)_2$. Some important bond lengths and distances are listed as show in Figure 3.3-3.6. Two transition state steps formation (**TS1**, **TS2**) with four-membered ring of monomer with initiators prior to ring-opening is found in all initiators. Like the case of CL with $Sn(O\text{-}nBut)_2$, the DFT structures of **Complex** for CL with $Sn(O\text{-}nHex)_2$ (Figure 3.3) and $Sn(O\text{-}nOct)_2$ (Figure 3.4) give the identical Sn-O^2 distance of 2.61 Å implying that longer chain does not affect the stability of **Complex** formation. For $Sn(O\text{-}iBut)_2$ (Figure 3.5) and $Sn(O\text{-}tBut)_2$ (Figure 3.6), the distances of Sn-O^2 slightly increase indicating that branching of R group does not affect the stability of the **Complex** either.

3.1.1.2 $Sn(O\text{-}nHex)_2$

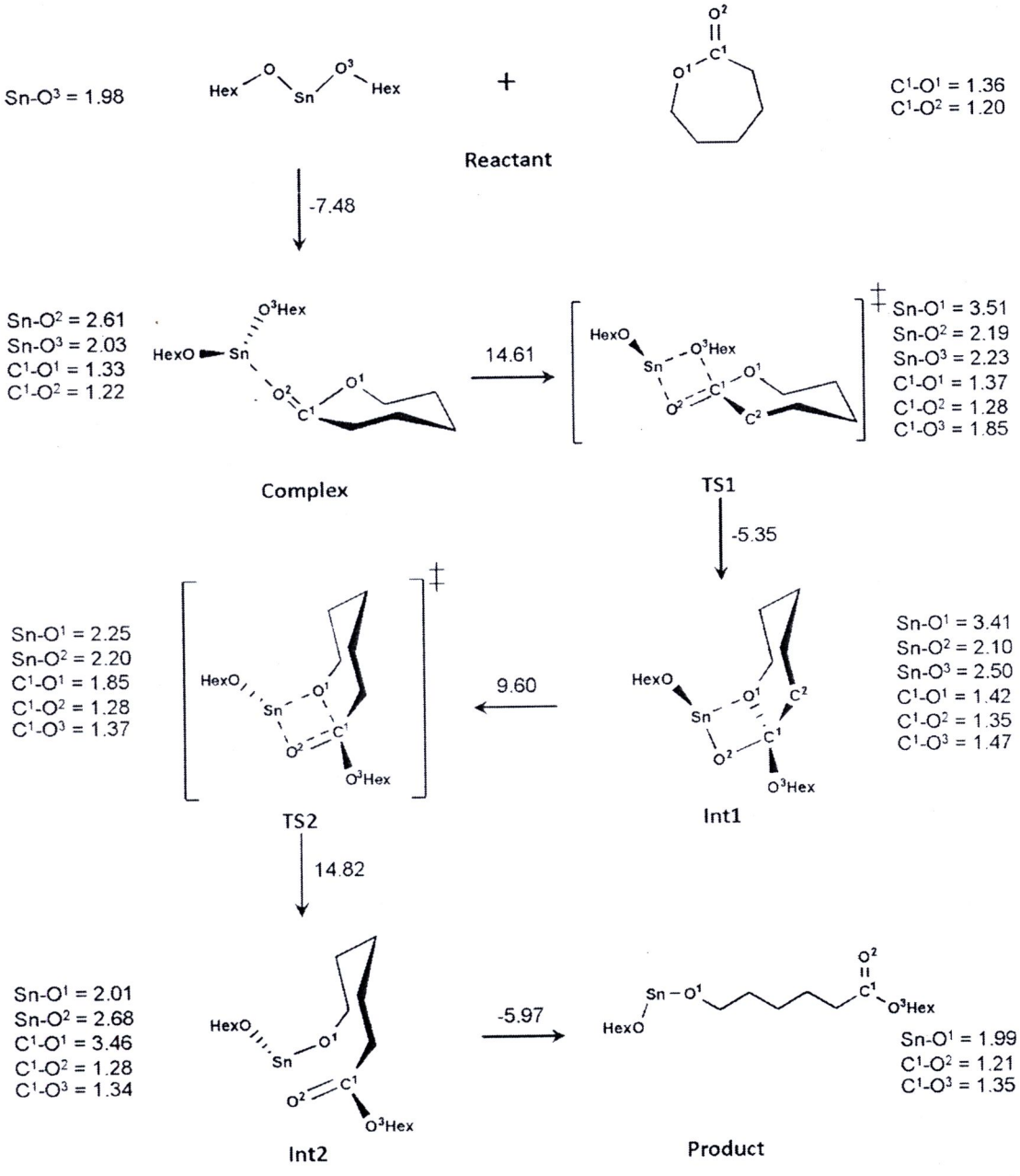

Figure 3.3 ROP mechanism of CL initiated with $Sn(O\text{-}nHex)_2$. Bond lengths are in Å and energies formation are in kcal mol^{-1}

3.1.1.3 $Sn(O\text{-}nOct)_2$

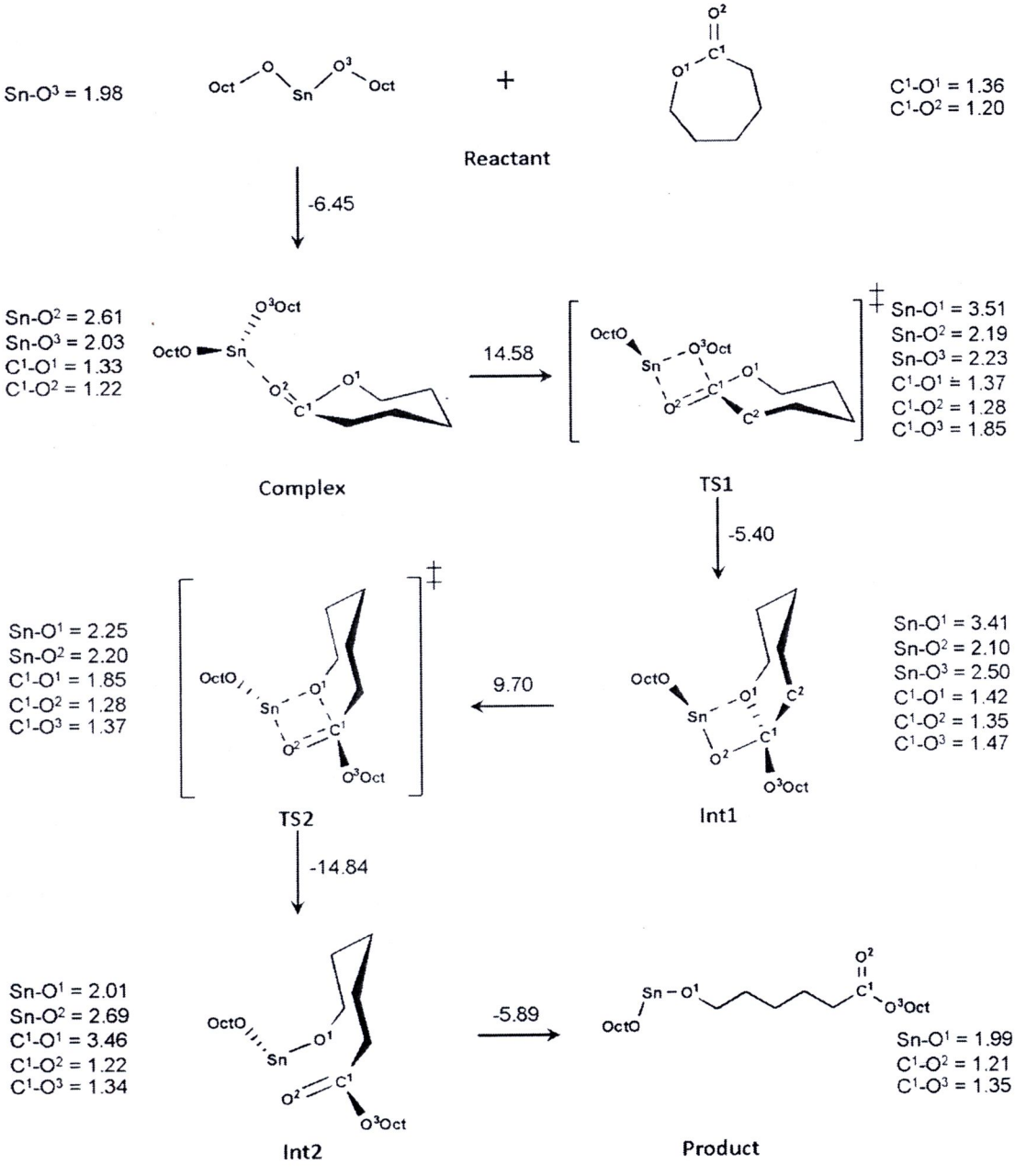

Figure 3.4 ROP mechanism of CL initiated with $Sn(O\text{-}nOct)_2$. Bond lengths are in Å and energies formation are in kcal mol^{-1}

3.1.1.4 Sn(O-iBut)$_2$

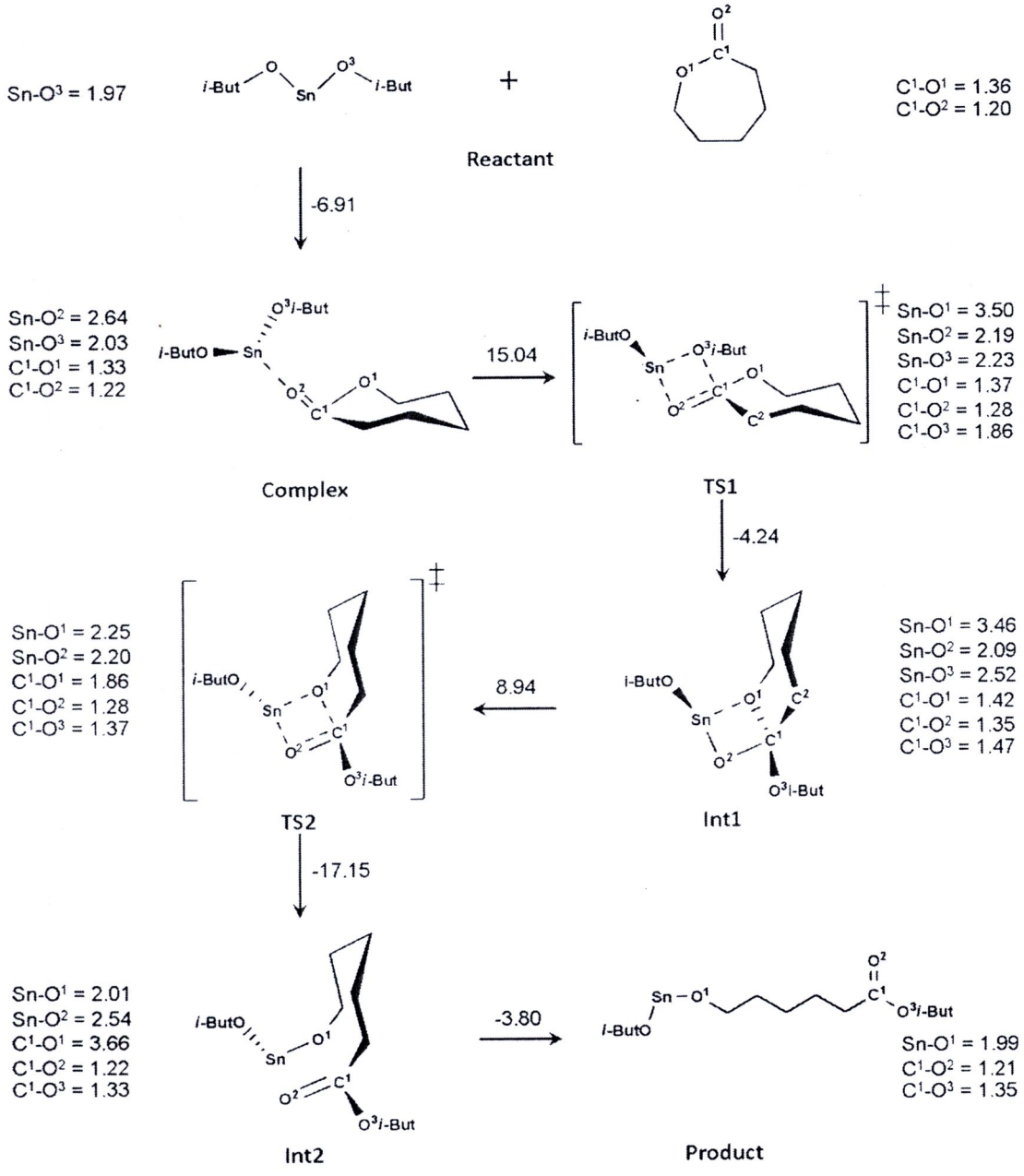

Figure 3.5 ROP mechanism of CL initiated with Sn(O-iBut)$_2$. Bond lengths are in Å and energies formation are in kcal mol^{-1}

3.1.1.5 $Sn(O\text{-}tBut)_2$

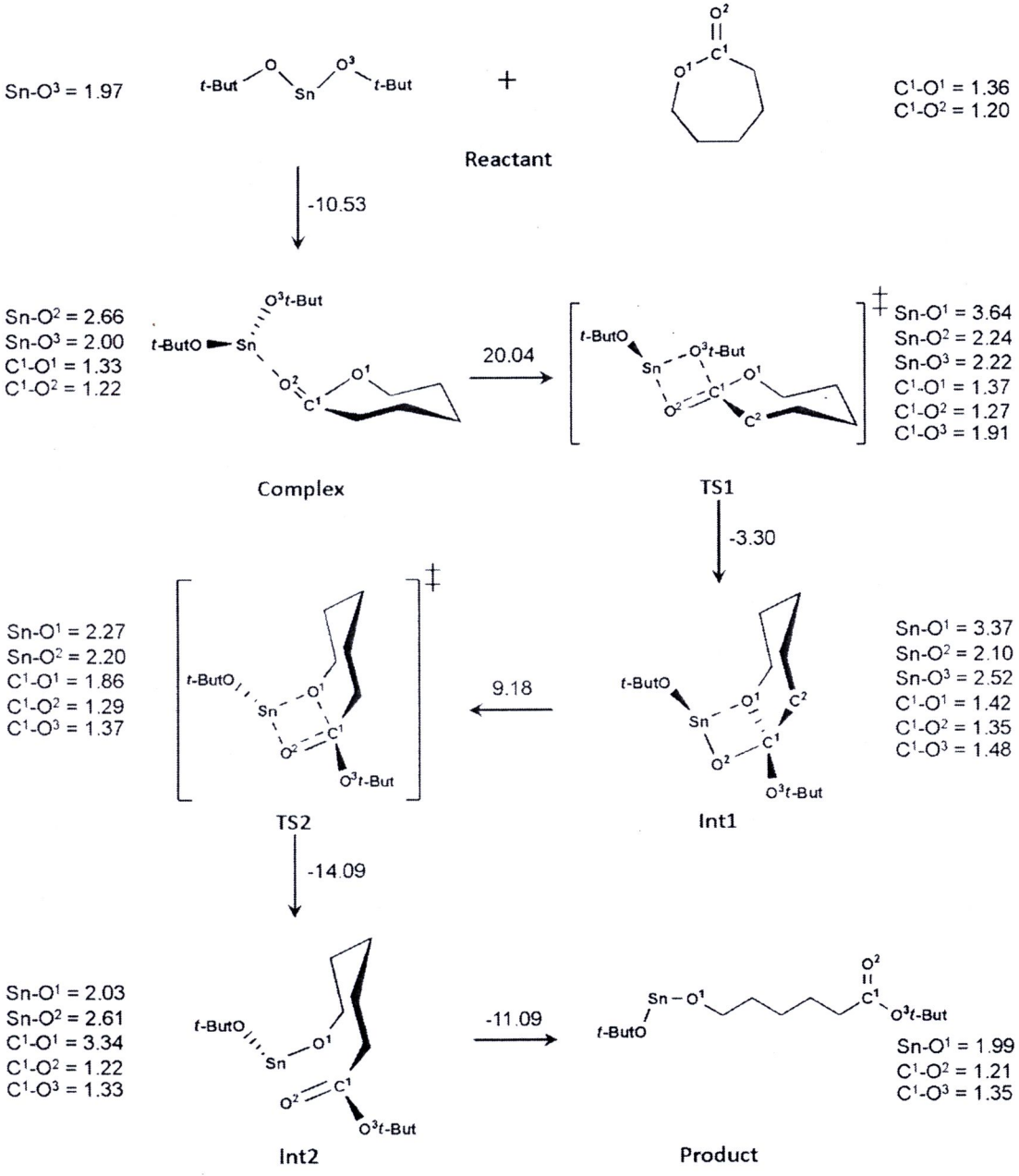

Figure 3.6 ROP mechanism of CL initiated with $Sn(O\text{-}tBut)_2$. Bond lengths are in Å and energies formation are in kcal mol^{-1}

The **Complex** stability is found in the following order of R group: *t*-But > *n*-But > *n*-Hex > *i*-But > *n*-Oct. The formation of **TS1** for all four initiators require moderate energy with the energy ranked as *t*-but> *i*-But = *n*-Oct > *n*-Hex > *n*-But which is order somewhat difference from **Complex** stability. This order of energy requirement may be explained with the stability of **TS1** by steric influence on the R group. The more bulky R group, the more energy is required for **TS1** to be formed. Note that *i*-But and *n*-Oct have the same steric effect even number of carbon atom on both are not the same. The confirmation of **TS1** formation with all initiators is proved with only one imaginary frequency.

The conversion of **TS1** to intermediate for all four initiators are proceeded similarly to the CL and $Sn(O\text{-}nBut)_2$. The rotation of $C^1\text{-}O^2$ bond causes the $Sn\text{-}O^3$ and $Sn\text{-}O^1$ distances to decrease and increase. The energy required for **TS2** to be formed is about 9.62 kcal mol^{-1} which is not much as required for **TS1** (values can be obtained by subtract the energy of **TS2** with **Int1**). The existences of **TS2** for all four initiators are confirmed by frequency calculation with one imaginary number and IRC. Like in the case of tin(II)-*n*-butoxide, **TS2** of these four initiators with driving force eventually rupture to **Int2** prior forming the product. The next cycle of ROP starts again when a new monomer comes close to CL and form **Complex**. And then, the propagation will be repeated to form a longer chain of polymer.

3.1.2 Natural bond orbital charge (NBO) analysis

Population analysis is a mathematical way of partitioning a wave function or electron density into charges on the nuclei, bond orders, and other related information. These are widely used to support the results that are not experimentally observable.

Atomic charges cannot be observed experimentally because they do not correspond to any unique physical property. In reality, atoms have a positive nucleus surrounded by negative electrons, not partial charges on each atom. However, condensing electron density and nuclear charges are on the nucleus resulting in understanding of the electron density distribution. Although this is an artificial assignment, it is very effective for predicting sites susceptible to nucleophilic or electrophilic attack and other aspects of molecular interaction. These partial charges correspond well to the chemist's view of ionic or covalent bonds, polarity, and so on.

For the accuracy of geometry calculation and confirm the purpose mechanism, NBO charges were used to discuss together. We found that, the result from structure optimization agrees well with NBO analysis in which NBO charge can be described the electron delocalization on each atom. For example in tin(II)-*n*-butoxide, the results of structure optimization in Figure 3.2 corresponding to the results of NBO in Figure 3.7. At the formation from Complex to **TS1**, the positive charge of Sn and C^1 increase due to the donating group of electron on O^2, O^1 resulting in the increasing of the negative charge on O^2, O^1 also more negative respectively. Meanwhile, the negative charge of O^3 was increased due to the long distance after taking place the transition structure.

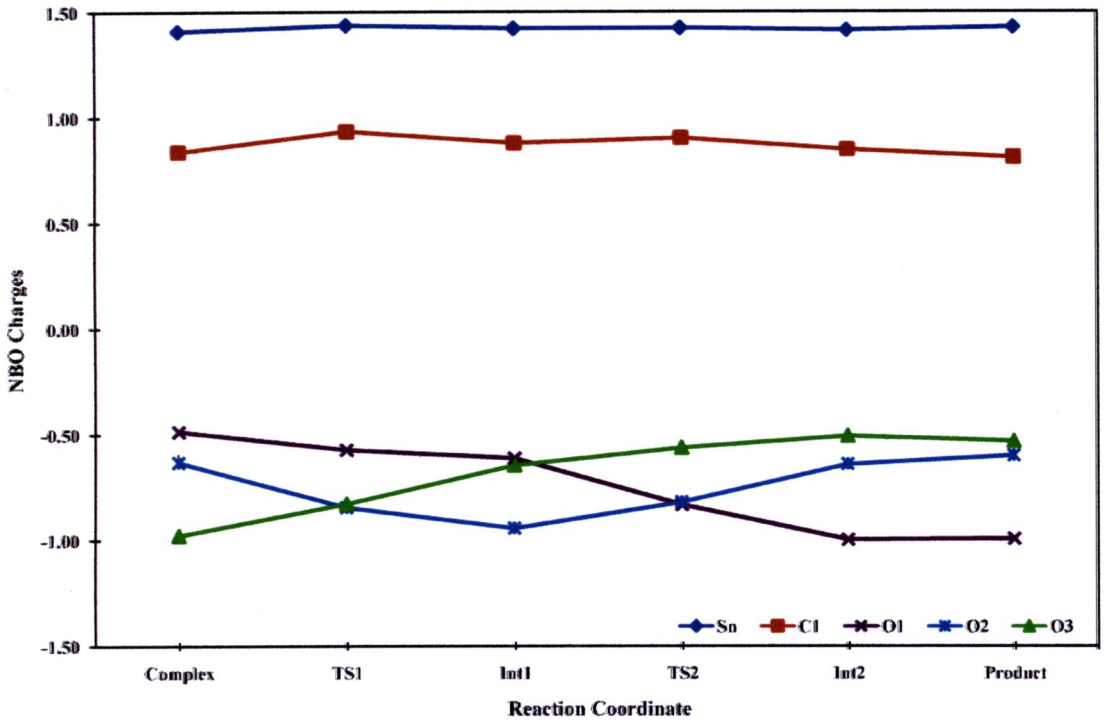

Figure 3.7 NBO charges of selected atoms involved in the reaction intermediates in the ROP of CL initiated by $Sn(O\text{-}nBut)_2$

As the same with the NBO charge analysis of other initiators of $Sn(O\text{-}nHex)_2$ in Figure3.8, $Sn(O\text{-}nOct)_2$ in Figure 3.9, $Sn(O\text{-}iBut)_2$ in Figure 3.10, and $Sn(O\text{-}tBut)_2$ in Figure 3.11 are similar with $Sn(O\text{-}nBut)_2$ result. All NBO charge results were support the purpose mechanism as well. The nucleophilic and electrophilic properties in each atom play an important role for interaction. Finally, the donor/acceptor electron caused to occuring the complete polymerization.

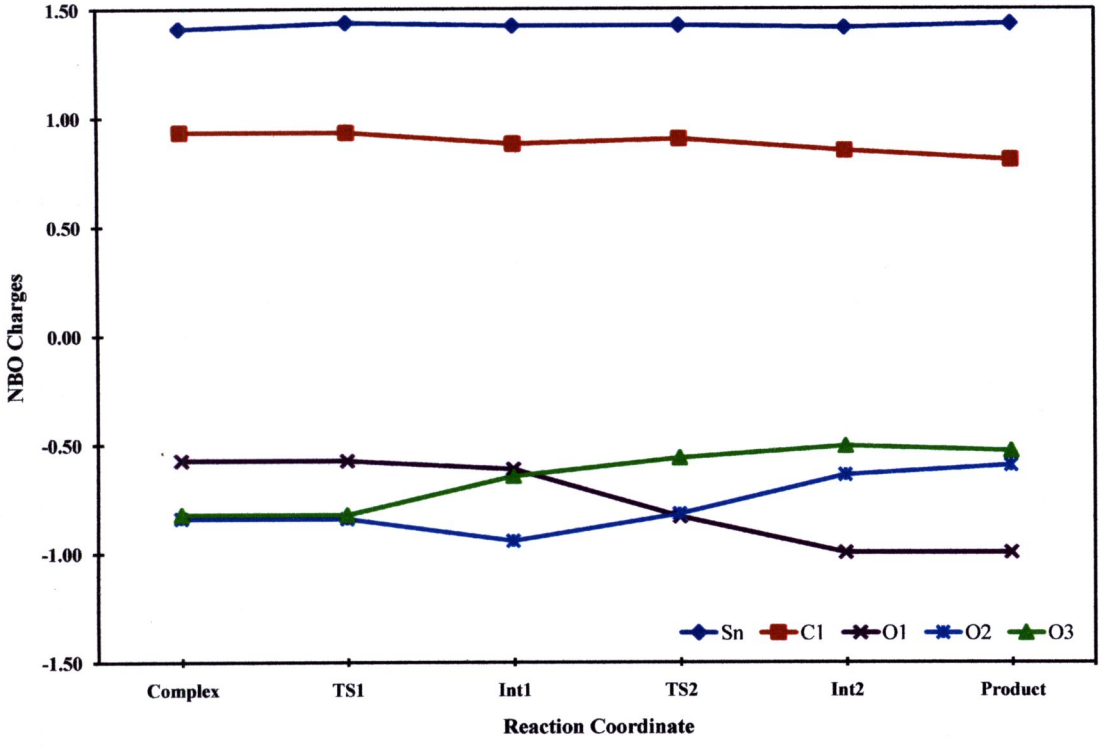

Figure 3.8 NBO charges of selected atoms involved in the reaction intermediates in the ROP of CL initiated by $Sn(O\text{-}nHex)_2$

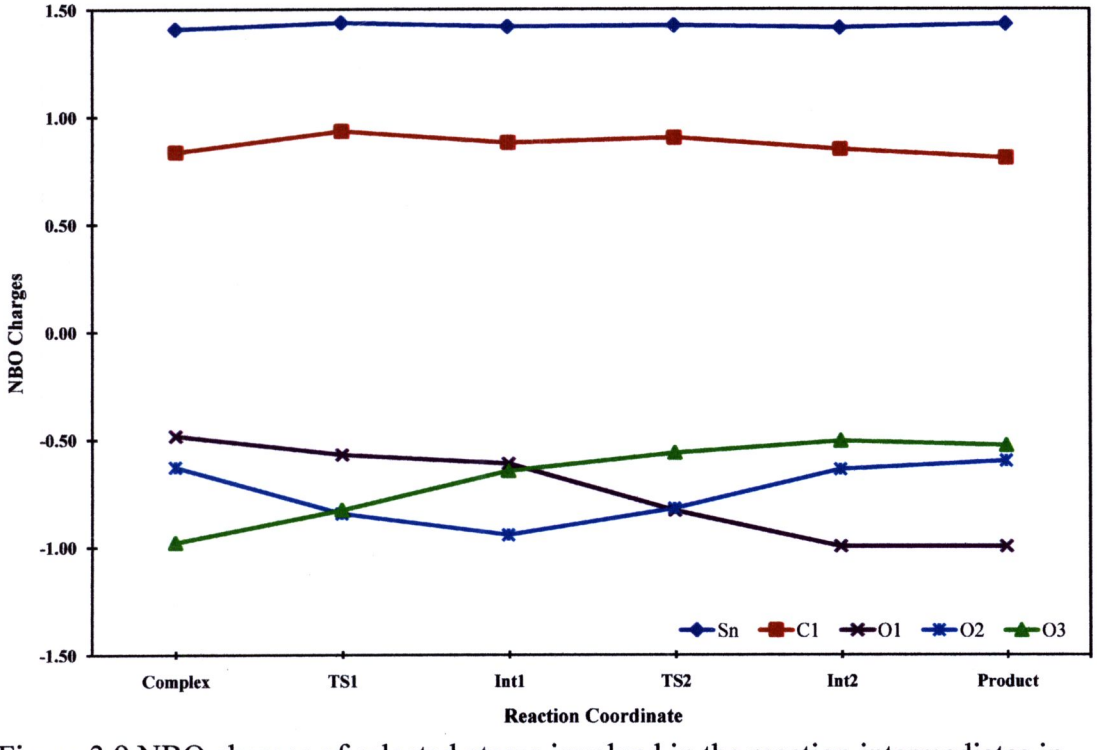

Figure 3.9 NBO charges of selected atoms involved in the reaction intermediates in the ROP of CL initiated by $Sn(O\text{-}nOct)_2$

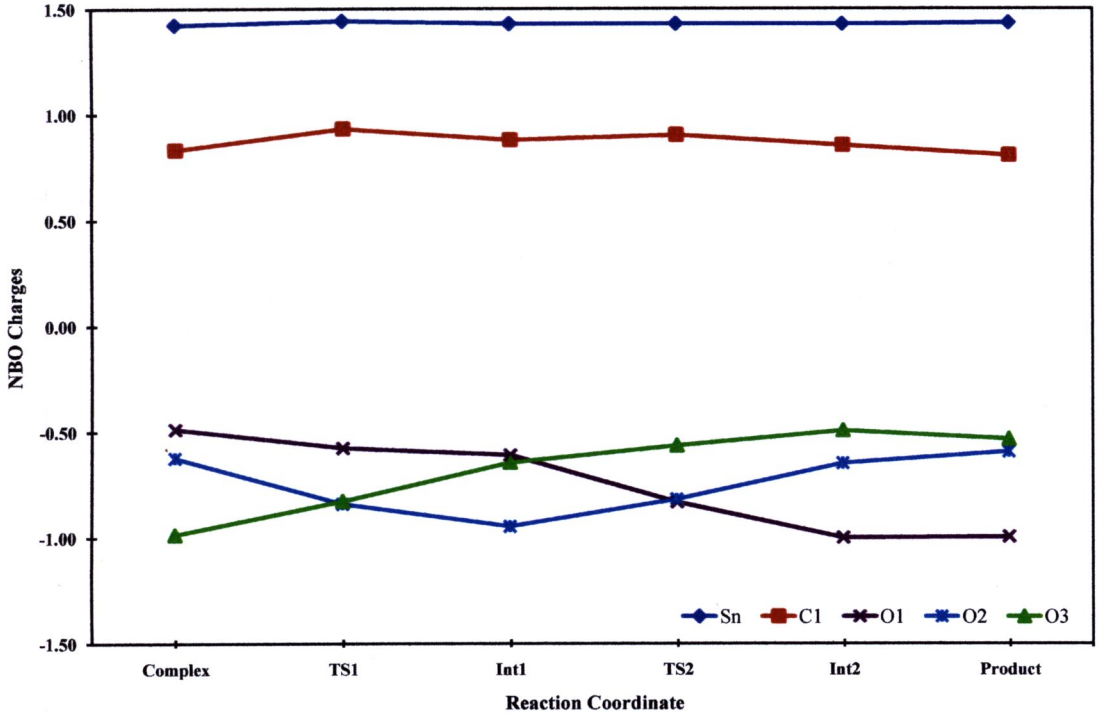

Figure 3.10 NBO charges of selected atoms involved in the reaction intermediates in the ROP of CL initiated by $Sn(O\text{-}iBut)_2$

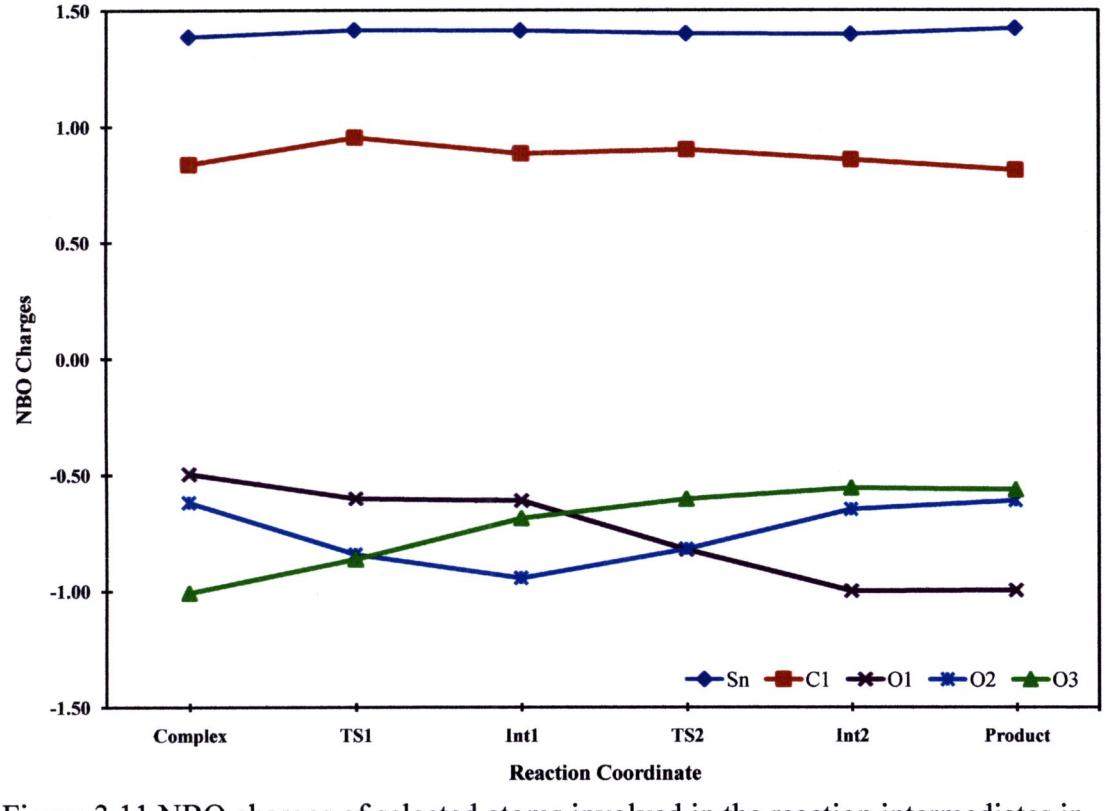

Figure 3.11 NBO charges of selected atoms involved in the reaction intermediates in the ROP of CL initiated by $Sn(O\text{-}tBut)_2$

3.1.3 Molecular orbital band gap analysis

In molecules, the possible electronic energies are discrete, quantized energy levels. As molecules become larger, these energy levels move closer together. We calculated molecular orbitals for estimate the band gap from the highest occupied molecular orbital (HOMO) and the lowest unoccupied molecular orbital (LUMO) energy separation. This energy separation becomes smaller as the molecule grows larger.

In this case, we considered the energy band gap at only **TS1** step because of this step is the rate controlling step of all reactions. From Figure 3.12, energy differences of HOMO and LUMO of each initiators show insignificant difference between 4.52-4.66 kcal.mol^{-1}. Even though the R groups of side chains are longer. In general, in term of electron delocalization may be discussed that if the delocalization occurs on electron rich, forming bond will be presented whereas the electron poor, the bond will be broken.

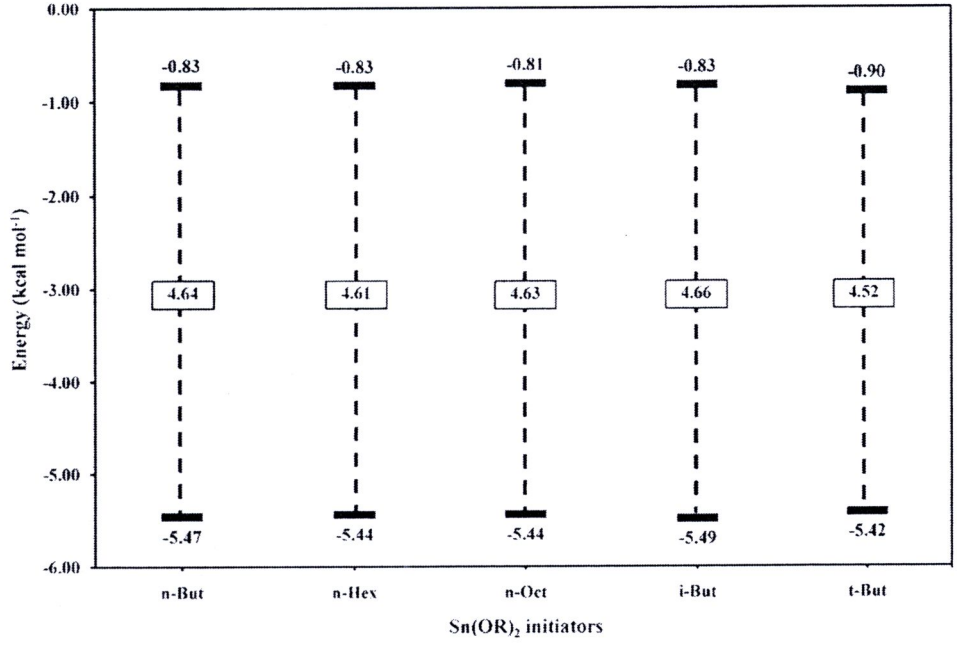

Figure 3.12 The energy differences of HOMO-LUMO band gap of each initiators

3.1.4 Intrinsic reaction coordination (IRC) analysis

For the accuracy of transition state geometry, the transition state structure was confirmed (normally confirmed by the motion of imaginary vibrational frequency) by the intrinsic reaction coordination (IRC) calculation. It is the use of steepest descent based algorithms for following a molecular reaction from a transition state towards and backward to a minimum point. The calculation is calculated by taking small steps along the negative gradient in a mass-weighted coordinate system.

In this thesis, the transitional state geometry at **TS1** of tin(II)-*n*-butoxide as shown in Figure 3.13. We considered only tin(II)-*n*-butoxide as an example result. The IRC was calculated at B3LYP/cc-pVTZ level for the present study. Figure 3.13 show the confirmation of transition structure of **TS1**, **TS2** molecule with **TS** is at the maximum point on the plot.

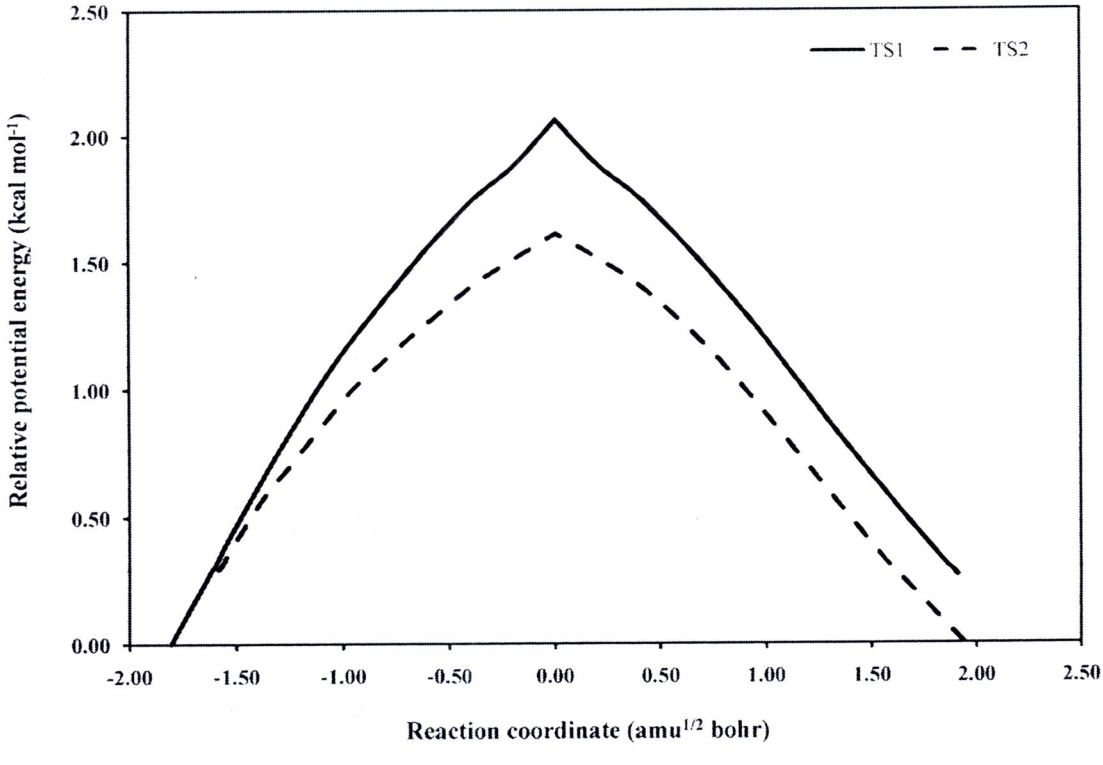

Figure 3.13 The IRC results of tin(II)-*n*-butoxide at **TS1** step

3.2 Energy minimization

In this section, we are especially interested in minimum points on the energy surface. Minimum energy arrangements of the atoms correspond to stable states of the system; any movement away from a minimum gives a configuration with a higher energy. There may be a very large number of minima on the energy surface. The minimum with the very lowest energy is known as the global energy minimum. To identify those geometries of the system that correspond to minimum points on the energy surface we use a minimization algorithm for finding the lowest energy. However, all molecules can never actually have this energy because it must always have some vibrational motion. Thus for the accurate energy calculation, we also computed the zero-point energy (ZPE) correction from the vibrational frequencies and added it to the total energy of the optimized geometry.

For this thesis, energy minimization was used to find the reaction energy in term of relative energy when compared to reactant energy on the pathway. The relative energies of all investigated stationary points (**Reactant**, **Complex**, **TS1**, **Int1**, **TS2**, **Int2** and **Product**) along the reaction profile for ROP mechanism of CL initiated by tin(II) alkoxide, $Sn(O\text{-}nBut)_2$, $Sn(O\text{-}nHex)_2$, $Sn(O\text{-}nOct)_2$, $Sn(O\text{-}iBut)_2$, and $Sn(O\text{-}tBut)_2$ are shown in Figure 3.12-3.16, respectively. The discussions about reaction energy of all initiators were discussed in sub section below.

3.2.1 $Sn(O\text{-}nBut)_2$

From energy profile of tin(II)-*n*-butoxide in Figure 3.14, the **Reactant** energy is assigned to be 0.00 kcal mol^{-1}. The **Complex** energy is lower than the **Reactant** energy about -7.53 kcal mol^{-1}. For **TS1**, the barrier height energy of this step is 14.58

kcal mol^{-1} and the **TS1** energy is 7.05 kcal mol^{-1} above **Reactant** energy. For the intermediate 1 (**Int1**), the energy is found to be 1.67 kcal mol^{-1} above the **Reactant** energy. The apparent barrier height of **TS2** step is 9.62 kcal mol^{-1} when compared with **Int1**. After the **TS2** state, the reaction energy decrease sharply at intermediate 2 (**Int2**) about -3.45 kcal mol^{-1} before to constant about -9.37 kcal mol^{-1} at the end of process that is **Product**. From the energy profile, the first transition state formation (**TS1**) is a rate determining step of this reaction.

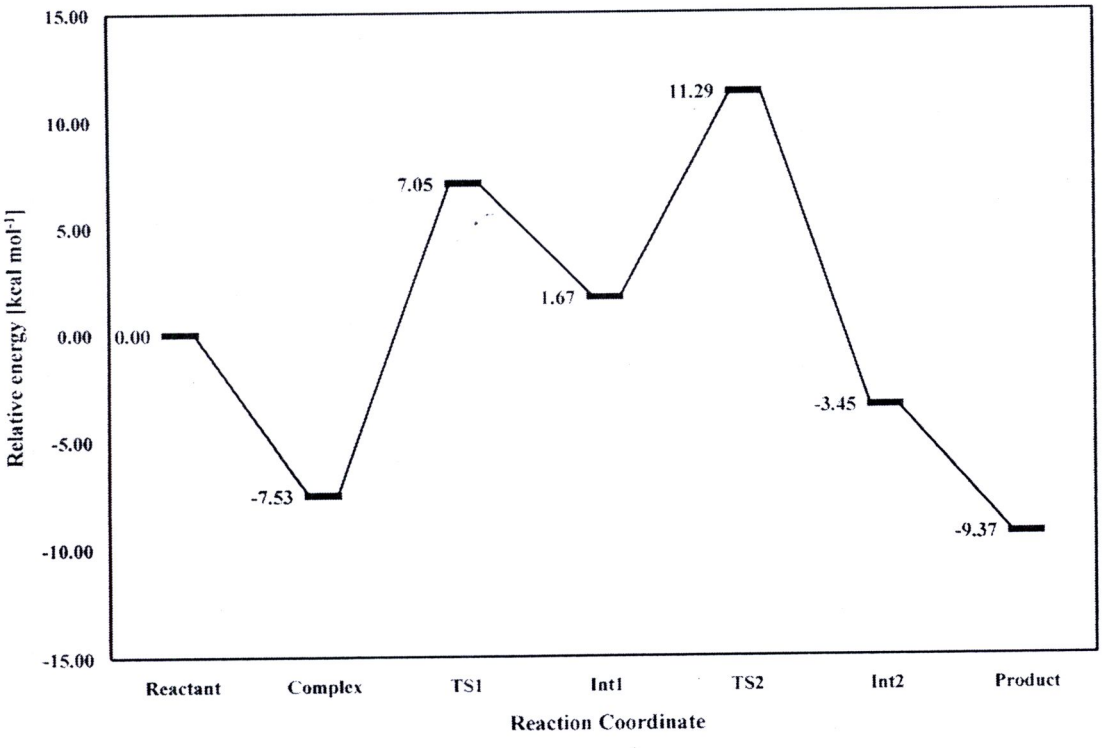

Figure 3.14 Relative energy profile for ROP of CL initiated by $Sn(O\text{-}nBut)_2$, calculated at B3LYP method

3.2.2 $Sn(O\text{-}nHex)_2$

From energy profile of tin(II)-*n*-hexoxide in Figure 3.15, the **Reactant** energy is assigned to be 0.00 kcal mol^{-1}. The **Complex** energy is lower than the **Reactant** energy about -7.48 kcal mol^{-1}. For **TS1**, the barrier height energy of this step is 14.61 kcal mol^{-1} and the **TS1** energy is 7.13 kcal mol^{-1} above **Reactant** energy. For the **Int1**, the energy is found to be 1.77 kcal mol^{-1} above the **Reactant** energy. The apparent barrier height of **TS2** step is 9.61 kcal mol^{-1} when compared with **Int1**. After the **TS2** state, the reaction energy decrease sharply at **Int2** about -3.45 kcal mol^{-1} before to constant about -9.42 kcal mol^{-1} at the end of process its call to be **Product**. From the energy profile, the first transition state formation (**TS1**) is a rate determining step of this reaction.

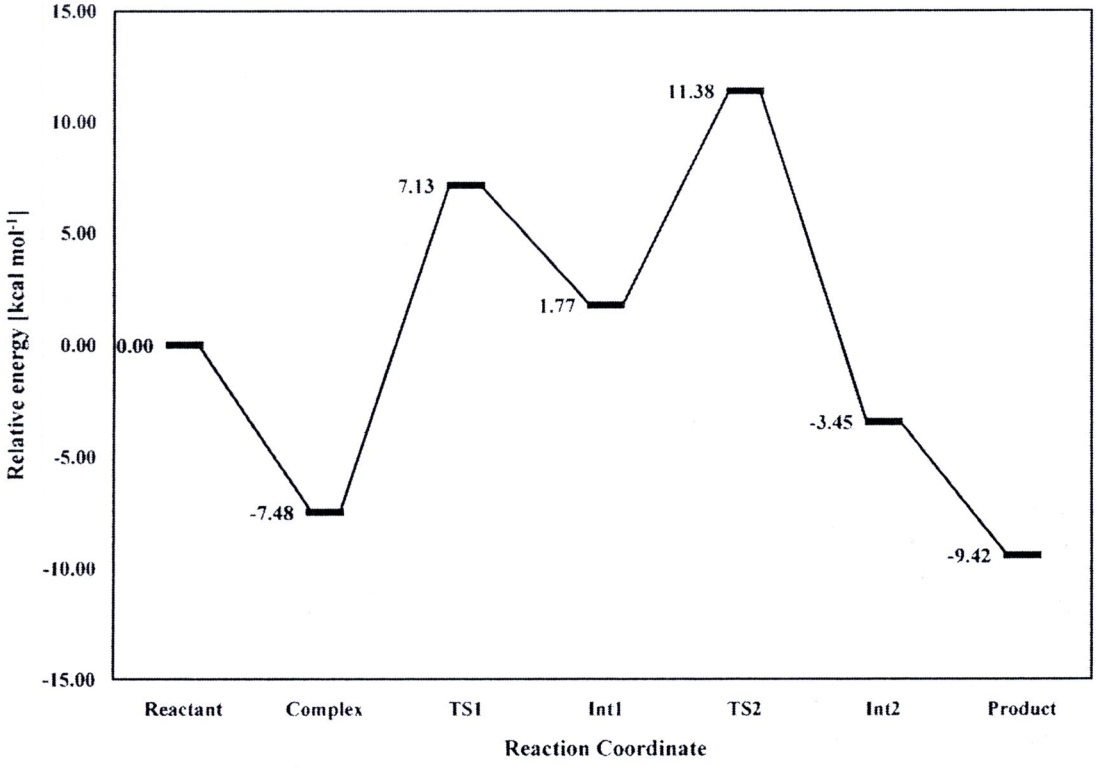

Figure 3.15 Relative energy profile for ROP of CL initiated by $Sn(O\text{-}nHex)_2$, calculated at B3LYP method

3.2.3 $Sn(O\text{-}nOct)_2$

From energy profile of tin(II)-*n*-Octoxide in Figure 3.16, the **Reactant** energy is assigned to be 0.00 kcal mol^{-1}. The **Complex** energy is lower than the **Reactant** energy about -6.46 kcal mol^{-1}. For **TS1**, the barrier height energy of this step is 14.59 kcal mol^{-1} and the **TS1** energy is 8.13 kcal mol^{-1} above **Reactant** energy. For the **Int1**, the energy is found to be 2.73 kcal mol^{-1} above the **Reactant** energy. The apparent barrier height of **TS2** step is 9.70 kcal mol^{-1} when compared with **Int1**. After the **TS2** state, the reaction energy decrease sharply at **Int2** about -2.41 kcal mol^{-1} before to constant about -8.30 kcal mol^{-1} at the end of process its call to be **Product**. From the energy profile, the first transition state formation (**TS1**) is a rate determining step of this reaction.

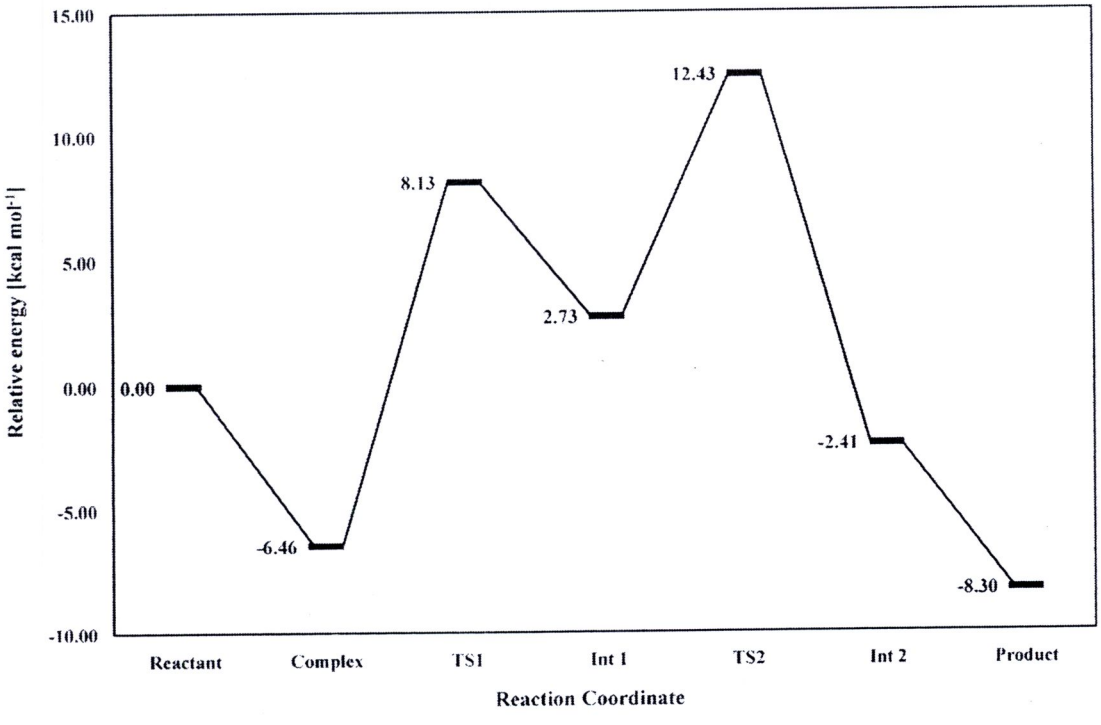

Figure 3.16 Relative energy profile for ROP of CL initiated by $Sn(O\text{-}nOct)_2$, calculated at B3LYP method

3.2.4 $Sn(O\text{-}iBut)_2$

From energy profile of tin(II)-*i*-Butoxide in Figure 3.17, the **Reactant** energy is assigned to be 0.00 kcal mol^{-1}. The **Complex** energy is lower than the **Reactant** energy about -6.91 kcal mol^{-1}. For **TS1**, the barrier height energy of this step is 15.04 kcal mol^{-1} and the **TS1** energy is 8.13 kcal mol^{-1} above **Reactant** energy. For the **Int1**, the energy is found to be 3.88 kcal mol^{-1} above the **Reactant** energy. The apparent barrier height of **TS2** step is 8.94 kcal mol^{-1} when compared with **Int1**. After the **TS2** state, the reaction energy decrease sharply at **Int2** about -4.33 kcal mol^{-1} before to constant about -8.13 kcal mol^{-1} at the end of process its call to be **Product**. From the energy profile, the first transition state formation (**TS1**) is a rate determining step of this reaction.

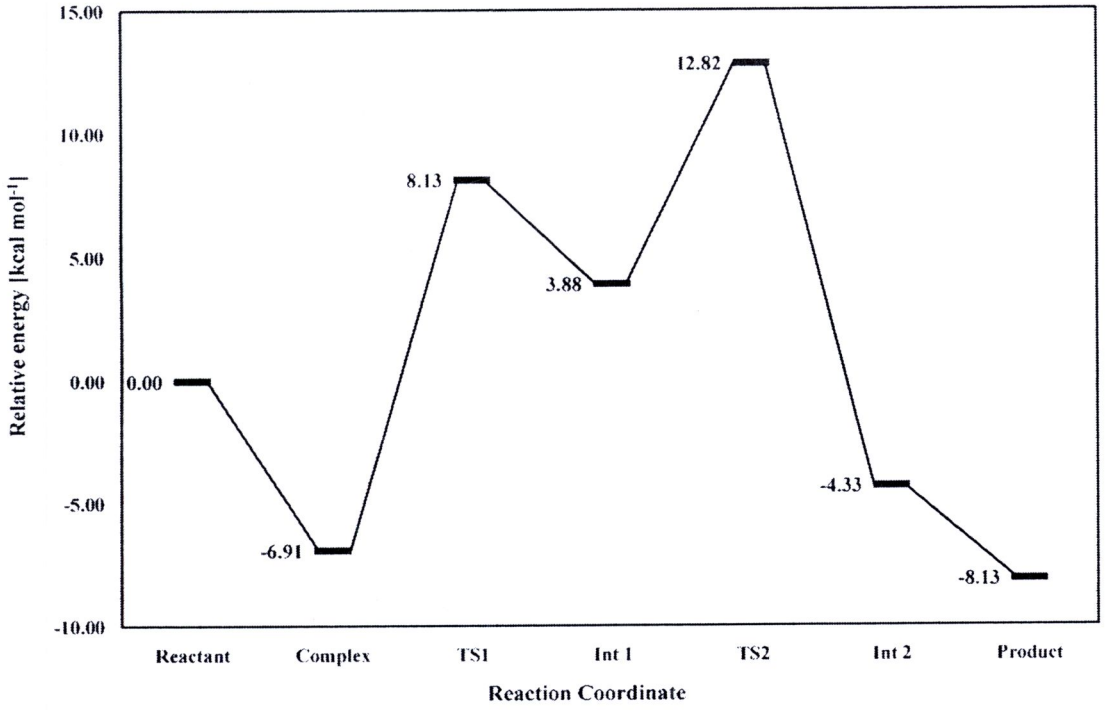

Figure 3.17 Relative energy profile for ROP of CL initiated by $Sn(O\text{-}iBut)_2$, calculated at B3LYP method

3.2.5 $Sn(O\text{-}tBut)_2$

From energy profile of tin(II)-*t*-Butoxide in Figure 3.18, the **Reactant** energy is assigned to be 0.00 kcal mol^{-1}. The **Complex** energy is lower than the **Reactant** energy about -10.55 kcal mol^{-1}. For **TS1**, the barrier height energy of this step is 20.04 kcal mol^{-1} and the **TS1** energy is 9.49 kcal mol^{-1} above **Reactant** energy. For the **Int1**, the energy is found to be 6.19 kcal mol^{-1} above the **Reactant** energy. The apparent barrier height of **TS2** step is 9.18 kcal mol^{-1} when compared with **Int1**. After the **TS2** state, the reaction energy decrease sharply at **Int2** about 1.28 kcal mol^{-1} before to constant about -9.81 kcal mol^{-1} at the end of process its call to be **Product**. From the energy profile, the first transition state formation (**TS1**) is a rate determining step of this reaction.

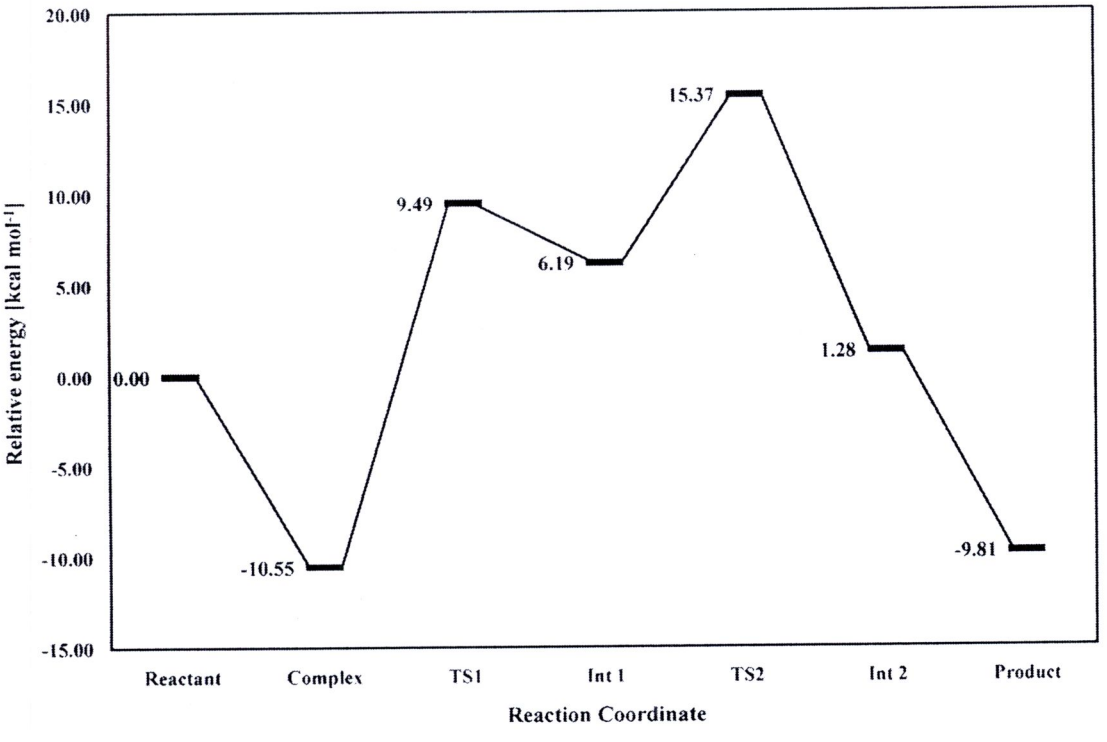

Figure 3.18 Relative energy profile for ROP of CL initiated by $Sn(O\text{-}tBut)_2$, calculated at B3LYP method

The calculated results were used to describe the ROP of CL initiated by different target initiators. From the results, the ROP mechanism of CL initiated by $Sn(O\text{-}nBut)_2$, $Sn(O\text{-}iBut)_2$, $Sn(O\text{-}tBut)_2$, $Sn(O\text{-}nHex)_2$ and $Sn(O\text{-}nOct)_2$ is found to be a coordination-insertion. There are 7 states and 6 steps of ROP mechanism along the reaction pathway. The details of ROP mechanism are found to be similar for all initiators including NBO charge analysis supporting. The reaction starts by a **Complex** formation of initiator and monomer. Then, a four-membered ring intermediate is formed via **TS1**. After that, bond breaking and bond forming of **TS2** yield the product. Finally, a propagation of PCL is achieved.

The relative energies of all stationary states are summarized again in Table 3.1. The energy comparison in each state of reactions shows that the longer chain, the more steric effect indicating that the energy in each state increases in the addition of number of carbon atom (C_4, C_6 and C_8) in initiator. In case of branching initiators; $Sn(O\text{-}nBut)_2$, $Sn(O\text{-}iBut)_2$ and $Sn(O\text{-}tBut)_2$, it is found that the more branching initiators the greater barrier height of **TS1**.

Table 3.1 The comparison of all relative energies state in ROP of CL initiated by tin(II) alkoxide series.

React. Coordination	Relative Energy (kcal mol^{-1})				
	n-But	*n*-Hex	*n*-Oct	*i*-But	*t*-But
Reactant	0.00	0.00	0.00	0.00	0.00
Complex	-7.53	-7.48	-6.46	-6.91	-10.55
TS1	7.05	7.13	8.13	8.13	9.49
Int 1	1.67	1.77	2.73	3.88	6.19
TS2	11.29	11.38	12.43	12.82	15.37
Int 2	-3.45	-3.45	-2.41	-4.33	1.28
Product	-9.37	-9.42	-8.30	-8.13	-9.81

The combination of energy profile is displayed in Figure 3.19 again. The energetic information was compared. At the **TS1**, the energy barrier heights of Sn(O-nBut)$_2$, Sn(O-nHex)$_2$, Sn(O-nOct)$_2$, Sn(O-iBut)$_2$ and Sn(O-tBut)$_2$ are 14.58, 14.61, 14.59, 15.04 and 20.04 kcal mol^{-1}, respectively. And at the **TS2**, the energy barrier heights of all initiators are 9.62, 9.61, 9.7, 8.94 and 9.18 kcal mol^{-1}, respectively. From the energy barrier height of both transition states, the energy of **TS1** is higher than energy of **TS2** indicating that the first transition state is a rate determining step of this reaction. **TS1** energy barrier height of tin(II)-*n*-butoxide is the lowest compared to other initiators. Therefore, tin(II)-*n*-butoxide will likely give the highest reaction rate compared to other initiators. And overall reaction of all initiators performed in exothermic.

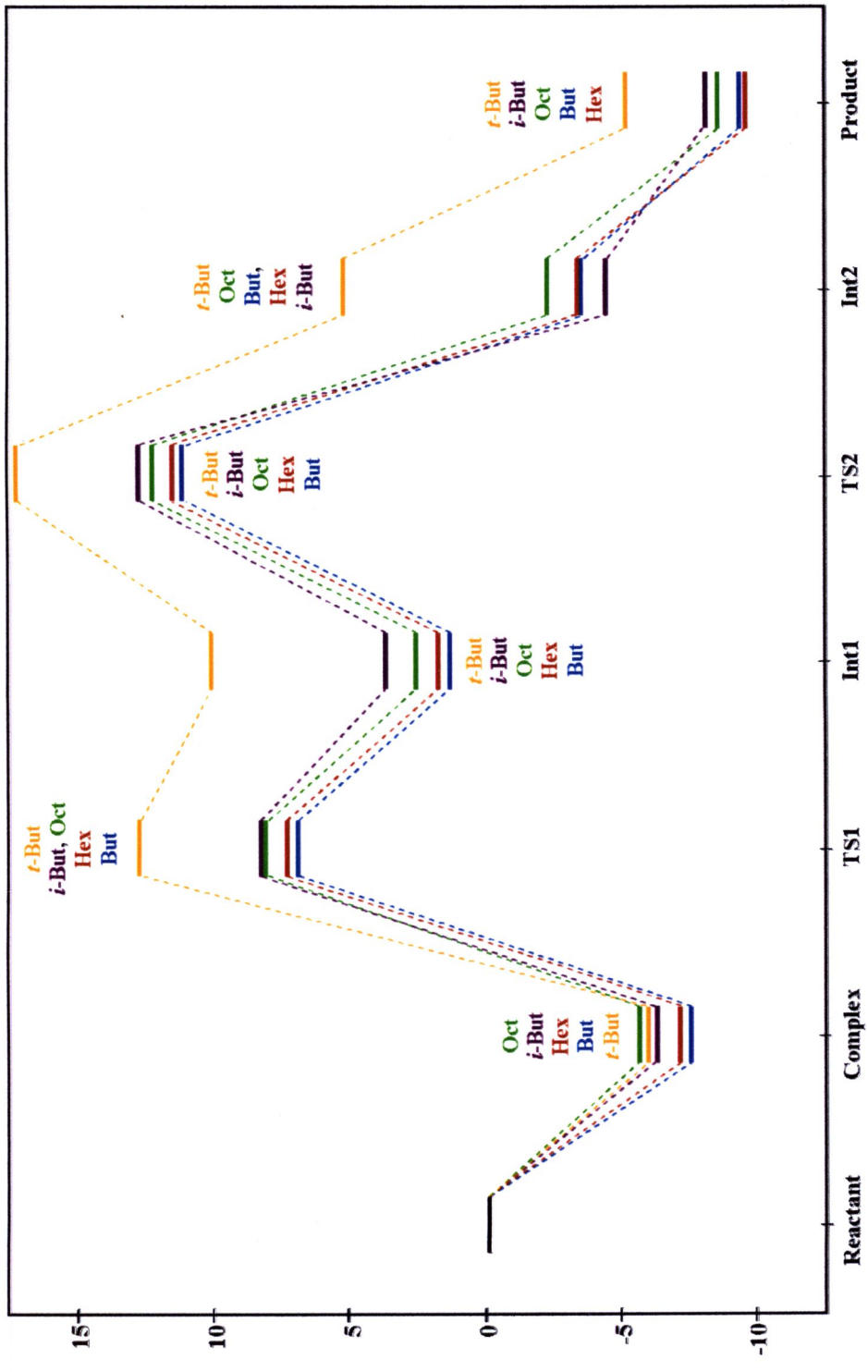

Figure 3.19 The combination of relative energy of all reactions in ROP of CL initiated by tin(II) alkoxide series

3.3 Kinetics rate reaction

The thermal rate constants in the range of 100-120 °C were calculated using information from the quantum calculation with TST implemented in TheRATE program. The calculated and experimental results are shown in Table 3.2 and plotted in Figure 3.20. Both available experiment and theoretical result correspond with TST in which the higher temperature, the faster rate constants becomes. Especially at 120 °C, the rate constants show the significant value. So, I will focus on this temperature.

Table 3.2 The theoretical and experimental rate coefficient of all initiators

$Sn(OR)_2$	Temperature (°C)	Rate coefficient (L mol^{-1} min^{-1})	
		Experiment [a]	Theory [b]
n-But	100	55.80	33.57
	110	111.70	45.01
	120	118.70	59.56
n-Hex	100	34.30	20.12
	110	62.70	27.01
	120	95.40	35.81
n-Oct	100	13.10	9.11
	110	16.30	12.67
	120	20.10	17.37
i-But	100	-	14.09
	110	-	19.67
	120	31.65[c]	27.05
t-But	100	-	1.56
	110	-	2.29
	120	9.90[c]	3.31

[a] Calculated by dilatometry's measurement of Punyodom's group [13].
[b] Calculated by TheRATE program of university of Utah [70, 71].
[c] This value were calculated by time number.

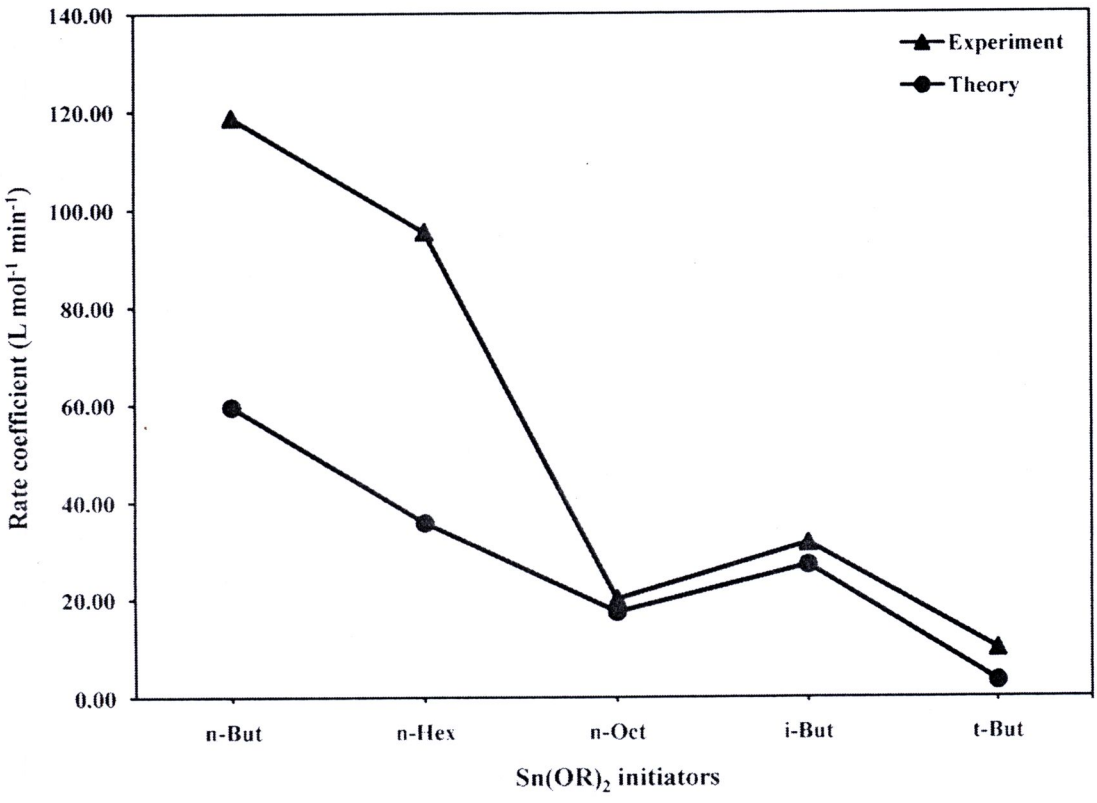

Figure 3.20 The rate coefficient of all reaction in ROP of CL initiated by tin(II) alkoxide series, calculated at 120 °C

Hence from experiment told us about the achievement of ROP synthesis with high MW at 120 °C. So, the comparisons of rate constants between the experiment (▲) and the calculation (●) results were discussed. From the comparison, we found that rate constant results show the interesting value. For experimental results, the rate constants of $Sn(O\text{-}nBut)_2$, $Sn(O\text{-}nHex)_2$, $Sn(O\text{-}nOct)_2$, $Sn(O\text{-}iBut)_2$ and $Sn(O\text{-}tBut)_2$ are 118.70, 95.40, 20.10, 31.65 and 9.90 L mol^{-1} min^{-1}, respectively. Meanwhile, the rate constants of all initiators in calculation results are 59.56, 35.81, 17.37, 27.05 and 3.31 L mol^{-1} min^{-1}, respectively. The calculated value is in good agreement within a factor of two compared with experimental data. Especially, tin(II)-*n*-butoxide shows the highest rate constants compared with the other initiators. It is indicated that tin(II)-

n-butoxide gives the highest reaction rate constant among the other initiators. This rate constant results are also related to the energy profile of tin(II)-*n*-butoxide (Figure 3.19) that is the lowest relative energy of rate determining step (**TS1**) compared to the other initiators.

From the discussion above, we found that rate constant results are different due to two main factors. Firstly, the effect of side chains, $Sn(O\text{-}nBut)_2$, $Sn(O\text{-}nHex)_2$, $Sn(O\text{-}nOct)_2$, shows that the longer chains, the more steric effect takes place indicating that the rate constant decreases as the number of carbon atom (C_4, C_6 and C_8) on R group of initiator increases. Secondly, the effect of branching initiators; $Sn(O\text{-}nBut)_2$, $Sn(O\text{-}iBut)_2$ and $Sn(O\text{-}tBut)_2$, it is found that the more branch of side chains, the more steric effect increases resulting in decreasing of rate constants.